University of Mississippi

eGrove

Honors College (Sally McDonnell Barksdale
Honors College)

2016

Calculating Liquefaction Potential of Northern Mississippi Using Shear Wave Data

Peshani Herath
University of Mississippi. Sally McDonnell Barksdale Honors College

Follow this and additional works at: https://egrove.olemiss.edu/hon_thesis

Part of the Physics Commons

CALCULATING LIQUEFACTION POTENTIAL OF NORTHERN MISSISSIPPI
USING SHEAR WAVE DATA

by
Peshani Herath

A thesis submitted to the faculty of The University of Mississippi in partial fulfillment of
the requirements of the Sally McDonnell Barksdale Honors College.

Oxford
May 2016

Approved by

_____
Advisor: Dr. Craig Hickey

_____
Reader: Dr. Zhen Guo

_____
Reader: Dr. Christopher Mullen

ACKNOWLEDGEMENTS

ABSTRACT

PESHANI HERATH: Calculating Liquefaction Potential of Northern Mississippi Using Shear Wave Data
(Under the direction of Dr. Craig Hickey)

The potential for liquefaction can be determined using the Liquefaction Potential Index (LPI). The LPI takes into account the thickness of the liquefiable layers and the factors of safety with respect to depth. This study creates a hybrid method for determining the LPI for different locations in Northern Mississippi. It calculates an average CSR for the region using existing borehole information. The CRR is then calculated using shear wave velocity profile data from a MASW survey. The LPI obtained from this process is compared to LPI values calculated using CPT data and borehole shear wave data. Surface shear wave velocity profiles are measured near two existing borehole locations, TNA013 and TNA012. The sites near borehole TNA013 and TNA012 are both very highly liquefiable according to the MASW method, but are only highly liquefiable using the borehole shear wave method. The LPI value calculated using CPT data near borehole TNA013 is classified as highly liquefiable and the LPI value near borehole TNA012 is classified as having a low liquefaction potential. The hybrid method gives a more conservative estimate of the liquefaction potential in the study area than the CPT method or borehole shear wave data.

TABLE OF CONTENTS

LIST OF TABLES

LIST OF FIGURES

1.0 Introduction

The Earth's crust is continuously moving atop a plastic layer called the asthenosphere. When this motion is hindered, strain can form in the lithosphere. This strain energy is released and manifests itself as an earthquake (Spall, 1977). Seismic activity can occur along plate boundaries (interplate) or in the interior of a tectonic plate (intraplate) (Lowrie, 1997). The majority of earthquakes originate from interplate seismic activity (Lowrie, 1997).

The seismic zones associated with interplate tectonics can be divided into those that follow mid-ocean ridges, continental plate boundaries, ocean-continent boundaries, and those caused by plates sliding by each other (Spall, 1977).

The processes that create intraplate earthquakes are more complex than those produced by plate boundaries and cannot be explained well through plate tectonics (Fillingim, 1999). One explanation for the existence of intraplate seismic activity is the zones of weakness in the Earth's crust. Weaknesses can arise from previous tectonic activities like failed ancient rift zones and passive margins deformed due to the development of active spreading centers. Over time, these zones can become incorporated into the central portion of a plate and remain inactive for many years. In the presence of stresses, these zones can get reactivated.

According to the United States Geological Survey, compared to the rest of the state Mississippi, the northern portion is the most at risk from an earthquake. This is due to the intraplate activity caused by the New Madrid Fault Zone (United States Geological

Survey, 2012). The New Madrid Seismic Zone is a compilation of several thrust faults that stretch from Arkansas to Illinois (Central United States Earthquake Consortium, 2016). It is the most active seismic area in the United States east of the Rocky Mountains (Missouri Department of Natural Resources, 2014). The New Madrid Seismic Zone encompasses northeastern Arkansas, southeastern Missouri, western Missouri, western Tennessee, southern Illinois, western Kentucky, southwestern Indiana, and northwestern Mississippi.

An ancient failed rift called the Reelfoot Rift underlies the Mississippi Embayment with a thick section of sedimentary rock filling the graben, or fault blocks located between two major faults, associated with the rift. The New Madrid Seismic Zone is located at the center of the buried rift (Braile *et al.*, 1986). The correlation of the earthquake epicenters with the buried rift complex indicates that the earthquakes in the New Madrid Seismic Zone are results of slippage along pre-existing zones of weakness. Contemporary stress fields going east to west in the New Madrid area reactivate these fault planes (Braile *et al.*, 1986).

Due to the harder, colder, drier and less fractured nature of the rocks, earthquakes in the central or eastern United States have a larger impact than earthquakes with similar magnitude in the western United States. They shake and damage a region 20 times larger than earthquakes in California (Missouri Department of Natural Resources, 2014). The effects of the New Madrid earthquake on December 1811 could be felt thousands of miles from the epicenter (United States Geological Survey, 2012). Three very large earthquakes occurred in 1811 – 1812 that are referred to as New Madrid earthquakes after a town in Missouri. The first principle earthquake that occurred in northeast Arkansas

December 16, 1811 was a magnitude 7.7. This was followed by a second primary shock in Missouri on January 23, 1812 with a magnitude of 7.5. The third principle shock was a magnitude 7.7 that occurred on February 7, 1812 along the Reelfoot fault in Missouri and Tennessee. Four aftershocks, each ranging in magnitude from 6.0 to 6.5 also occurred during this period. A report by Otto Nuttli states that more than 200 moderate to large aftershocks occurred in the New Madrid region between December 16, 1811 and March 15, 1812 (United States Geological Survey, 2012).

The primary cause of destruction in modern earthquakes is the collapse of manmade structures (Missouri Department of Natural Resources, 2014).In addition to the shaking from surface waves, damage to structures can occur when the foundation liquefies. Liquefaction is the tendency of an unconsolidated saturated soil to behave like a liquid when introduced to a shock, commonly an earthquake (Rauch, 1997). Liquefaction potential is related to the amount of subsurface ground water and its proximity to the surface, the soil type, and the magnitude and of the seismic activity at a given location. Liquefaction of soils is largely dependent on the Cyclic Stress Ratio (CSR), the measure of earthquake loading, and Cyclic Resistance Ratio (CRR), liquefaction resistance of the ground (University of Washington, 2016).

Liquefaction resistance of soils can be evaluated using several methods. The earliest and simplest method is based on the Standard Penetration Test (SPT). Later methods included the Cone Penetration Test (CPT), and small strain shear wave velocity (V_s) measurements (Andrus*et al.*, 2003). Because of the poor repeatability and inherent difficulties associated with the Standard Penetration Test, the CPT is used as a method to determining CRR for clean and silty sands (Robertson and Wride, 1998).

The Cone Penetration Test (CPT) can be useful in characterizing sites with discrete stratigraphic horizons or discontinuous lenses. It is valuable in accessing subsurface stratigraphy associated with soft material, discontinuous lenses, potentially liquefiable material, and landslides. In this method, a 1.41 inch diameter 55° to 60° cone is pushed through the underlying ground at a rate of 1 to 2 centimeters per second (Rodgers, 2004). A computerized log of the tip and sleeve resistance, induced pore pressure behind the cone tip, pore pressure ratio, and a lithologic interpretation of every two centimeter interval are produced. The tip resistance of a cone is related to the undrained shear strength of a saturated cohesive material while the sleeve friction is related to the friction of the horizon being penetrated. The higher the tip resistance, the less likely liquefaction will occur (Robertson and Wride, 1998).

Seismic waves can also be measured during a CPT. As a borehole is created using this technique a cone with seismic capabilities, seismic cone, can detect shear waves (Song and Mikell, 2013). The borehole shear wave velocity is an alternative method to determine liquefaction. Unlike the penetration tests, this measurement is better in gravelly soils and capped landfills (Andrus *et al.*, 2003). In addition to use in liquefaction studies, multiple studies have established that shear-waves in the upper 30 to 60 meters can greatly affect surface ground motion duration and amplification of an earthquake. The average shear wave velocity in the top 30 m, known as Vs30, is the metric obtained from the shear wave velocity profile to correlate with amplification (Odum, 2007).

A shear wave velocity profile can also be measured using surface refraction and multichannel analysis of surface waves, MASW, methods. Multichannel analysis of surface waves is becoming more popular in geotechnical studies and measures the speed

of the surface waves. The seismic waves are produced by impacting the ground with a sledgehammer. This energy is detected by a multiple channel recording system and a receiver array that is spread out over hundreds of meters. A dispersion curve (surface wave velocity versus frequency) is then calculated from this data and inverted to obtain a shear wave versus depth profile (Park, 2007).

The potential for liquefaction can be determined using the Liquefaction Potential Index (LPI). The LPI takes into account the thickness of the liquefiable layers and the factors of safety with respect to depth. The purpose of this study is to create a hybrid method for determining the LPI for different locations in Northern Mississippi. The hybrid method uses an average CSR for the region calculated using existing borehole information. The local CRR is calculated using a shear wave velocity profile obtained from a MASW survey. This hybrid method would not require additional CPT or boreholes. In order to evaluate the feasibility of this hybrid method, the LPI is calculated using CPT following the method of Song and Mikell (2013). Then, an average CSR is calculated using all the borehole data in the region and the LPI is recalculated using the average CSR. The viability between the two LPI values is less than ten percent. The LPI is then calculated using shear wave velocity from boreholes and compared to the CPT derived LPI. There was no discernable pattern between the two calculations. The LPI values calculated using the borehole shear wave method are generally higher (more liquefiable) than the LPI values using CPT data. The LPI using shear wave velocity and Vs30 measured at the various boreholes are also compared. These values correlated with low velocities indicating high liquefaction potentials. Surface shear wave velocity profiles are measure at two borehole locations using the MASW survey method. These

two shear wave profiles are used to calculate a LPI value using the average CSR as well as the Vs30 value. The site near borehole TNA013 is very highly liquefiable according to the MASW method and highly liquefiable using the borehole shear wave method. It has a soil type of D according to Vs30 values. The site near borehole TNA012 is very highly liquefiable using MASW data and highly liquefiable using borehole shear wave data. It is classified as soil type E according to the Vs30 values.

2.0 Liquefaction

In general, liquefaction is used to refer to all the failure mechanisms due to pore pressure build-up during cyclic shear of undrained, saturated soil. When subjected to shearing stresses, loose saturated soil grains tend to be rearranged into to a denser packing. When this occurs, there is less space and the water in the pore space is forced out. However, the pore pressure will increase as the shear load increases if the drainage of the pore water is obstructed. This transfers the stress from the soil skeleton to the pore water, and can lead to the reduction of effective stress and shear resistance of the soil. When the shear resisting stress is less than the driving shear stress, the soil undergoes deformation, or liquefaction (Rauch, 1997).

When loose, or contractive soil, is sheared monotonically, it reaches peak shear strength and softens to a residual shear resistance (top Figure 1a). Liquefaction flow failure occurs when the static driving stress exceeds the residual shear resistance (Rauch, 1997).When this same soil is sheared cyclically, excess pore pressure is generated with each load cycle (middle Figure 1a). Without pore water drainage, the pore pressure increases causing the system to move towards failure. If the static driving stress is greater than the shear strength, flow failure occurs and continues even after the cyclic load is removed. In order for liquefaction to occur where the shear resistance is overcome by the static driving load, a contracting saturated soil must undergo sufficient undrained stress for an adequate number of load cycles. A great amount of damage can be caused with this

process before equilibrium conditions are reestablished at the reduced shear strength (Rauch, 1997).
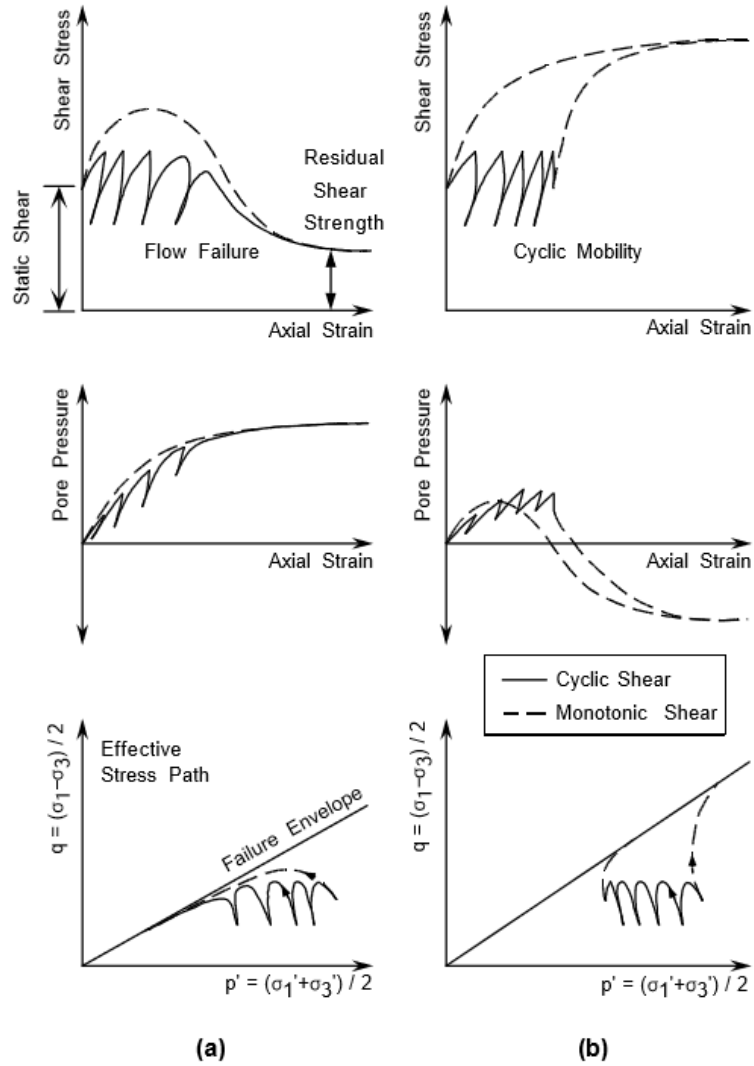
Figure 1. Response of **a)** contractive **b)** dilative saturated sand to undrained shear.

When dense, or dilative, soil is sheared, some pore pressure will be produced with small strains. If the strain is large, however, the pore pressure will decrease. The soil grains will move on top of each other, increasing in volume, or dilating. Monotonic shearing in dense soils cause an increase in effective stress and shear resistance (Rauch,

8

1997). When the same soil is dynamically loaded, each load cycle will generate some pore pressure, resulting in deformation (middle Figure 1b). At a certain point, however, further strain is prevented by the tendency of the soil to increase in volume. Flow failure does not occur in undrained dilative soil during cyclic loading because the shear strength remains greater than the static diving shear stress. This behavior is called cyclic mobility (Rauch, 1997).

P. K. Robertson and C. E. Fear in 1996 suggested a classification system to define soil liquefaction. The two major categories are flow liquefaction and cyclic softening. Flow liquefaction is used for saturated, undrained flow of a contractive, or loose, soil when static residual stress exceeds the residual shear strength of the soil (Rauch, 1997). Cyclic softening is used for undrained dilating soils that experience large deformation during cyclic shearing due to pore pressure build up. This category can be further divided into cyclic liquefaction and cyclic mobility. Cyclic liquefaction describes the condition when cyclic shear stresses are greater than the initial static shear stress, creating a stress reversal. This can produce a stress reversal where a condition of zero effective stress can be present during which large deformation can occur (Rauch, 1997). Cyclic mobility is where deformation is accumulated in each cycle of shear stress where conditions of zero effective stress do not develop (Rauch, 1997).

Loose, saturated, shallow deposits of cohesionless soils that produce strong ground motion during large magnitude earthquakes are most susceptible to liquefaction (Rauch, 1997). Liquefaction and large deformation are more common with soils that are compressive as opposed to dilative that tend to experience cyclic softening and limited

9

deformation. Unsaturated soils do not experience liquefaction because pore pressure is not generated when the soil volume is decreased (Rauch, 1997).

Liquefaction causes soil grains to rearrange themselves. Anything that hinders this motion will increase the resistance of a soil to liquefaction. Factors related to the geologic formation of the deposit like particle cementation, soil fabric, and aging can hinder the process of rearranging grains (Rauch, 1997). The stress history of a soil can also affect the liquefaction potential. Deposits with uneven consolidation conditions, for example, are more resistant to pore pressure generation. Soils that have been over-consolidated are less likely to experience liquefaction because they have been exposed to greater static pressure, reducing the likelihood of the grains rearranging themselves (Rauch, 1997). Soils buried deeper than approximately 15 meters are more resistant to liquefaction because the effective overburden pressure increases with depth. This is because the frictional resistance between the grains is proportional to the effective confining stress (Rauch, 1997).

The characteristics of the soil grains such as shape, size distribution, and composition also influence the liquefaction susceptibility. Generally, sands and silt are most susceptible to liquefaction, but there are records of gravel liquefying. Well graded, angular sand particles are less likely to experience liquefaction because the interlocking of the grains is more stable. Silty sand, however, are prone to liquefaction because they are deposited loosely. Rounded grains with uniform size distribution are most susceptible to liquefaction (Rauch, 1997).

Clays with measureable plasticity can hinder the movement of grains during cyclic shearing. This impedes the generation of pore pressure, reducing liquefaction.

Liquefaction is rarely observed in soils with a large quantity of plastic fines because the adhesion created between the grains impedes the larger particles from moving into a denser arrangement. Non-plastic fines, however, contribute to liquefaction because they are inherently collapsible and inhibit the drainage of excess pore pressure (Rauch, 1997).

The permeability of the soil is another parameter controlling liquefaction. Soils that are less permeable cannot transport pore fluids and cause pore pressure to build up during cyclic loading. The permeability of the surrounding rock will also influence liquefaction susceptibility. Permeable layers above and below a saturated soil can help dissipate the excess pore water, decreasing pore pressure. This high permeability is why gravelly soils are less prone to liquefaction (Rauch, 1997).

Liquefaction does not occur in places at random; rather, they are controlled by a certain geologic and hydrologic environment (Greene and Youd, 1994). Relatively younger, looser soils deposited in an area with high ground water levels provides the optimum conditions for liquefaction. Areas with the ground water table within ten meters of the ground surface tend to be areas with the most abundant occurrences of liquefaction (Greene and Youd, 1994). The opportunity of liquefaction occurring is restricted by the frequency of earthquake occurrence and the intensity of seismic ground shaking. Seismic source zones must be taken into account if a liquefaction opportunity map is to be developed. Seismic motion is more intense the closer the site is to the source of the disturbance, and will increase the opportunity for liquefaction (Greene and Youd, 1994).

Even if the soil has the necessary characteristics for liquefaction to occur, it will not occur until the proper stress or ground motion from earthquakes is present. The primary factors controlling how the surface soil behaves in the presence of an earthquake

are shear wave velocity, depth to hard rock, and non-linear dynamic material properties (Silva, 2003).

Multiple studies (Borcherdt and Gibbs, 1976; Joyner *et al.*, 1981; Seed *et al.*, 1988) have established that shear-waves in the upper 30 to 60 meters can greatly affect surface ground motion duration and amplification of an earthquake. Shallow Vs is referred to as Vs30 (Odum, 2007). The average Vs is calculated using velocity versus depth profile to a depth of 30 meters (Odum, 2007) using the equation,

$$V_S 30 = \frac{\sum_{i=1}^{n} d_i}{\sum_{i=1}^{n} \frac{d_i}{V_{si}}} \tag{1}$$

where V_{si} is the velocity of the ith layer and d_i is the thickness of the ith layer between 0 to 30 meters (Odum, 2007).

The velocity at which the soils transmit shear waves can contribute to the amplification of motion. Ground shaking is stronger when the shear wave velocity is lower. Table 1 shows the five soil types defined by the National Earthquake Hazards Reduction Program based on their shear wave velocities (USGS, 2012). High amplification can lead to liquefaction. Therefore, soils that have high amplification may also be susceptible to liquefaction.

The chart organizes soils ranging from least amount of amplification to the greatest amount of amplification. Soil type E will experience the strongest ground motion and soil type A will contribute least to ground motion amplification. S-waves travel faster in hard rock than in soft soil (Odum, 2007). Soft soils amplify shear waves, so the ground shaking in these areas are enhanced. Thin layers of soft soils that overlay stiffer soils or bed rock, however, will behave as if the site were lying on stiff soil. Areas that have endured earthquakes before will also experience greater ground motion during future

earthquakes. In order for the liquefaction of a site to be accurately evaluated the characteristics of the soil, the magnitude and intensity of the earthquake, the hydrology of the environment, and its proximity to an earthquake hazard zone must all be taken into account (USGS, 2012).

Table 1. Classification of Soil Types Based on NEHRP Shear Wave Velocities

Soil Type	Shear Wave Velocity (m/s)	Rock/Soil Description
A	> 1500	Hard Rock (includes unweathered intrusive igneous rocks): do not contribute greatly to shaking amplification
B	1500 - 750	Bed Rock: do not contribute greatly to shaking amplification
C	750 - 350	Dense Soil/ Soft Rock(includes) mudstones, sandstones, and limestone
D	350 - 200	Stiff Soil (includes mud, sands, gavels ad silts): significant amplification of shaking
E	< 200	Soft Soil (include water-saturated mud and artificial fill): the strongest amplification of shaking

Source: United States Geological Survey. "Soil Type and Shaking Hazard in the San Francisco Bay Area." *Soil Type and Shaking Hazard in the San Francisco Bay Area*. U.S. Geological Survey, 2012.

2.1 Calculating Liquefaction Potential

The potential for liquefaction can be determined using the Liquefaction Potential Index (LPI). The definition of LPI as defined by Iwasaki *et al.* (1978) is a method to characterize liquefaction hazard (Holzer *et al.,* 2009). Though other definitions for LPI were proposed, redefining it could alter the interpretations and the significance of an LPI value. The LPI takes into account the thickness of the liquefiable layers and the factors of safety with respect to depth. In order to calculate the LPI, Iwasaki *et al.* (1978) assumed

that the severity of liquefaction is related to the total thickness of the liquefied layers, the depth of these layers (proximity to the surface), and how much less the liquefaction factor of safety (FS) is to one. The FS is a measure of the soil's capacity to resist liquefaction during an earthquake (Holzer *et al.,* 2009). The LPI is defined as,

$$LPI = \int_0^{20} F_L \times w(z)dz \tag{2}$$

$$w(z) = 10 - 0.5z \tag{3}$$

$$F_L = 1 - FS \quad for\ FS \leq 1 \tag{4}$$

$$F_L = 0 \quad for\ FS > 1 \tag{5}$$

where z is the depth in meters and $w(z)$ is a weighting factor that can vary from ten at the surface to zero at 20 meters. Theoretically the value of the LPI can range from zero to 100 (Holzer *et al.,* 2009). Table 2 lists the soil classification in terms of the liquefaction potential index.

Table 2. Liquefaction Potential Index

Liquefaction Potential Index Value	Liquefaction Potential Classification
LPI≤2	Low
2<LPI≤5	Moderate
5<LPI≤15	High
LPI>15	Very High

Source: Song, C. R., and Mikell, N. "Earthquake and Piping Hazard Assessment for Desoto, Tunica, and Tate County, Mississippi." Department of Civil Engineering, University of Mississippi, 2013.

The liquefaction potential is quantified using the Cyclic Resistance Ratio (CRR) and Cyclic Stress Ratio (CSR). CRR represents dimensionless cyclic strength and CSR represents dimensionless cyclic stress induced by an earthquake. The likelihood of liquefaction occurring in terms of Cyclic Resistance Ratio for different ground layers is determined using the Factor of Safety equation (Song and Mikell, 2013),

$$FS = \frac{CRR}{CSR}(MSF) \tag{6}$$

FS is the Factor of Safety and MSF is the earthquake Magnitude Scaling Factor. The MSF is determined using Table 3.

Table 3. Magnitude Scaling Factor

Earthquake Magnitude	Magnitude Scaling Factor
5.5	2.20
6.0	1.76
6.5	1.44
7.0	1.19
7.5	1.00
8.0	0.84
8.5	0.72

Source: Song, C. R., and Mikell, N. "Earthquake and Piping Hazard
        Assessment for Desoto, Tunica, and Tate County, Mississippi."
        Department of Civil Engineering, University of Mississippi, 2013.

When the FS is greater than or equal to one, liquefaction will not occur; if the FS is less than one, liquefaction can occur (Johari and Khodaparast, 2013).

Liquefaction resistance of soils can be evaluated using the Standard Penetration Test (SPT), the Cone Penetration Test (CPT), and small strain shear wave velocity (V_s) measurements (Andrus *et al.*, 2003). Each method has its advantages and disadvantages. The calculation of CSR, however, is the same for all three methods.

The Cyclic Stress Ratio (CSR) is calculated using the equation,

$$CSR = 0.65 \frac{a_{max}}{g} \frac{\sigma_{v0}}{\sigma_{v0}'} r_d \qquad (7)$$

where a_{max} is the peak ground acceleration in percent g (g = 9.81 m/s), σ_{v0}' is the effective vertical stress, σ_{v0} is the total vertical stress, and r_d stress reduction factor. The a_{max} value is obtained using the peak ground acceleration map (PGA) in Figure 2. "Peak ground acceleration is a measure of the maximum force experienced by a small mass located at the surface of the ground during an earthquake (USGS, 2014)." It is an index to hazard for short stiff structures during an earthquake. A PGA map is generated by assigning an annual probability of occurrence to a ground motion associated with a certain magnitude from a particular distance (USGS, 2015). This study will use an a_{max} value of 0.2g because the peak ground acceleration in the study is about 20 percent (Song and Mikell, 2013).

The total vertical stress is calculated using the equation,

$$\sigma_{v0} = \sum \gamma_t z \qquad (8)$$

where γ_t is the total unit weight of the soil and z is the depth in meters (Song and Mikell, 2013). For the Cone Penetration Test, the total unit weight is calculated using the equation,

$$\gamma_t = 11.46 + 0.33 \log(z) + 3.10 \log(f_s) + 0.70 \log(q_t) \qquad (9)$$

where z is the depth in meters, q_t (kPA) is the tip resistance corrected for pore water pressure, and f_s (kPA) is the local friction measured from the CPT (Song and Mikell, 2013). The corrected tip resistance is calculated using,

$$q_t = q_c + u_2(1 - a_n) \tag{10}$$

where q_c is the tip resistance measured during the CPT, u_2 is the pore pressure measured behind the cone, and a_n is the net area ratio. Typically, the a_n value is between 0.7 and 0.8. In sands, q_c can be used in equation 10 instead of q_t. This study will be using q_c because the pore pressure behind the cone is unknown (Song and Mikell, 2013).
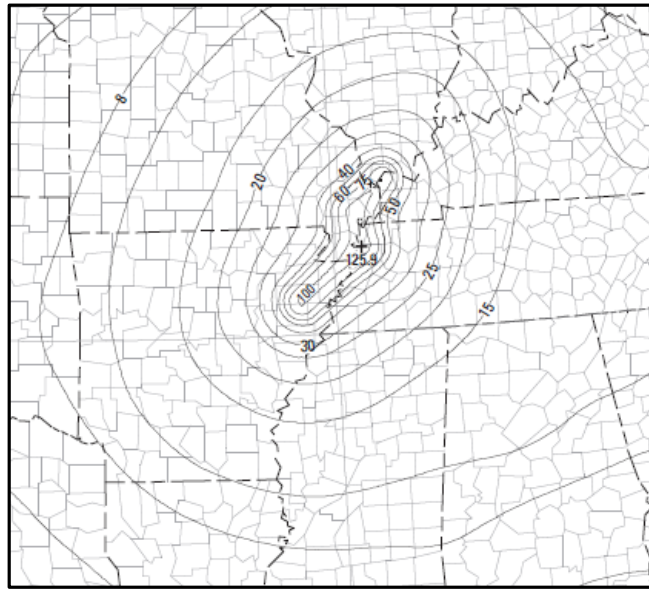

Figure 2. Map of peak ground acceleration in percent g (Song and Mikell, 2013).

The effective stress is calculated using the equation,

$$\sigma'_{vo} = \sigma_{v0} - p \tag{11}$$

where p is the pore water pressure calculated using the equation,

$$p = \gamma(z - z_0) \tag{12}$$

17

where z is the depth in meters, z_0 is the depth of the water table, and γ is the unit weight

of water (9.81 kN/m^3). This study assumes the water table to be at one meter below the

surface (Song and Mikell, 2013).

The stress reduction factor is evaluated using the following guide lines,

$$if\, z \leq 9.15\, meters \qquad r_d = 1.0 - 0.00765z \qquad (13)$$

$$if\, 9.15 < z \leq 23\, meters \qquad r_d = 1.174 - 0.0267z \qquad (14)$$

$$if\, 23 < z \leq 30\, meters \qquad r_d = 0.744 - 0.008z \qquad (15)$$

$$if\, z > 30\, meters \qquad r_d = 0.5 \qquad (16)$$

where z is the depth in meters (Song and Mikell, 2013).

2.1.1 Determining Factor of Safety Using the Standard Penetration Test (SPT)

In the SPT method, blows from a slide hammer are used to drive a standard

thick-walled sample tube into the ground at the bottom of a deep narrow hole, borehole;

the slide hammer has standard weights and fall distance. The sample tube is driven up to

18 inches into the ground and the number of blows needed to penetrate every six inches is

recorded (geotechdata.info, 2013). The SPT blow count value is the sum of the number of

blows needed for the second and third six inches of penetration; it is also called the

standard penetration resistance and the N-value. This value indicates the relative density

of the subsurface soil and can be used to estimate the approximate shear strength

properties of the soil (geotechdata.info, 2013).

The CRR for an earthquake with a 7.5 magnitude is obtained using SPT results

by,

$$CRR_{7.5} = \frac{1}{34 - N_{1,60cs}} + \frac{N_{1,60cs}}{135} + \frac{50}{(10N_{1,60cs} + 45)^2} - \frac{1}{200} \qquad (17)$$

18

$N_{1,60cs}$ is the clean sand equivalent of the overburden stress corrected SPT blow count,

$$N_{1,60cs} = a + bN_{1,60} \tag{18}$$

a and b are coefficients that account for the effects of the fines content (FC) (Johari and Khodaparast, 2013),

$$a = 0 \quad\quad \text{FC} \leq 5\% \tag{19}$$
$$a = e^{[1.76 - (190/\text{FC2})]} \quad\quad 5\% < \text{FC} < 35\% \tag{20}$$
$$a = 5.0 \quad\quad \text{FC} \geq 35\% \tag{21}$$

$$b = 1 \quad \text{FC} \leq 5\% \tag{22}$$
$$b = [0.99 + (\text{FC}^2/1000)] \quad\quad 5\% < \text{FC} < 35\% \tag{23}$$
$$b = 1.2 \quad \text{FC} \geq 35\% \tag{24}$$

and $N_{1,60}$ is the corrected SPT blow count normalized to the effective overburden stress of 100 kPa.

2.1.2 Determining Factor of Safety Using Cone Penetration Test (CPT)

CPT penetration resistance has been proposed as an alternative method to determining CRR for clean and silty sands due to the poor repeatability and inherent difficulties associated with the Standard Penetration Test (Robertson and Wride, 1998). The CPT uses data retrieved while the cone pushes through the underlying ground to calculate the liquefaction potential of a soil. The tip resistance (q_c) of a cone and sleeve friction (f_s) are used calculate the friction ratio (F). F is used to classify a soil based upon its reaction to the cone being forced through the soil. High ratios represent clayey material while low ratios represent sandy material. Sands typically have a ratio less than 1% and most soils typically don't exceed 20% ratio (Rodgers, 2004).

Using CPT measurements, the Cyclic Resistance Ratio for a 7.5 magnitude

earthquake is calculated using the expressions,

$$CRR_{7.5} = 93 \left(\frac{(q_{c1N})_{cs}}{1000}\right)^3 + 0.08, \quad if\ 50 \le (q_{c1N})_{cs} \le 160 \tag{25}$$

$$CRR_{7.5} = 0.833 \left(\frac{(q_{c1N})_{cs}}{1000}\right) + 0.05, \quad if (q_{c1N})_{cs} < 50 \tag{26}$$

where $(q_{c1N})_{cs}$ is the clean-sand equivalent normalized cone penetration resistance (Song

and Mikell, 2013). It is calculated using the equation,

$$(q_{c1N})_{cs} = K_c Q \tag{27}$$

where K_c is the correction factor for grain characteristics and Q is the normalized cone

resistance (Song and Mikell, 2013). Q is calculated with the following equation,

$$Q = \frac{(q_c - \sigma_{vo})}{100} C_N \tag{28}$$

where C_N is the normalization factor for cone penetration resistance (CPR) (Song and

Mikell, 2013). This factor is calculated using the equation,

$$C_N = \left(\frac{100}{\sigma'_{vo}}\right)^n \tag{29}$$

where 100 represents one atmospheric pressure in kPa and n is an exponent that varies

with soil type (Song and Mikell, 2013). K_c is calculated using the conditions,

$$if\ I_c \le 1.64, \quad K_c = 1.0 \tag{30}$$

$$if\ 1.64 < I_c < 2.36\ and\ F < 0.5\%, \tag{31}$$

$$K_c = -0.403 I_c{}^4 + 5.581 I_c{}^3 - 21.63 I_c{}^2 + 33.75 I_c - 17.8$$

$$if\ 1.64 < I_c < 2.60, \tag{32}$$

$$K_c = -0.403 I_c{}^4 + 5.581 I_c{}^3 - 21.63 I_c{}^2 + 33.75 I_c - 17.88$$

$$if\ I_c \ge 2.70 \quad CRR = 0.053 Q K_\alpha \tag{33}$$

where K_α is a correction factor to account for shear stress (Song and Mikell, 2013).I_c in the above expression is calculated using the equation,

$$I_c = \sqrt{[(3.47 - logQ)^2 + (1.22 + logF)^2]} \qquad (34)$$

where F is the normalization friction ratio. It is calculated using the equation,

$$F = \frac{f_s}{(q_c - \sigma_{vo})} 100 \qquad (35)$$

The stress component n is calculated with respect toI_c. The criteria for this value are expressed as,

$$if\, I_c \leq 1.64, \quad n = 0.5 \qquad (36)$$

$$if\, 1.64 < I_c < 3.30, \quad n = (I_c - 1.64)0.3 + 0.5 \qquad (37)$$

$$if\, I_c \geq 3.30, \quad n = 1.0 \qquad (38)$$

$$if\, \sigma'_{vo} > 300\, KPa \quad n = 1.0 \qquad (39)$$

This system of equations must be iterated until the change in n is less than 0.01 (Song and Mikell, 2013).

The left side of the Figure 3 is a graph of the CRR versus corrected CPT tip resistance for a magnitude 7.5 earthquake (Robertson and Wride, 1998). The filled in markers represent liquefaction while the blank markers represent no liquefaction. Soils susceptible to liquefaction tend to fall on the left side of the limiting shear strain line, and no liquefaction markers are denser on the right side of the line. The higher the tip resistance, the less likely liquefaction will occur. The right side of Figure 3 is the same graph different with soil types denoted. Silty sand to sandy silt is plotted on the far left, followed by silty sand and clean sand on the far right (Robertson and Wride, 1998).
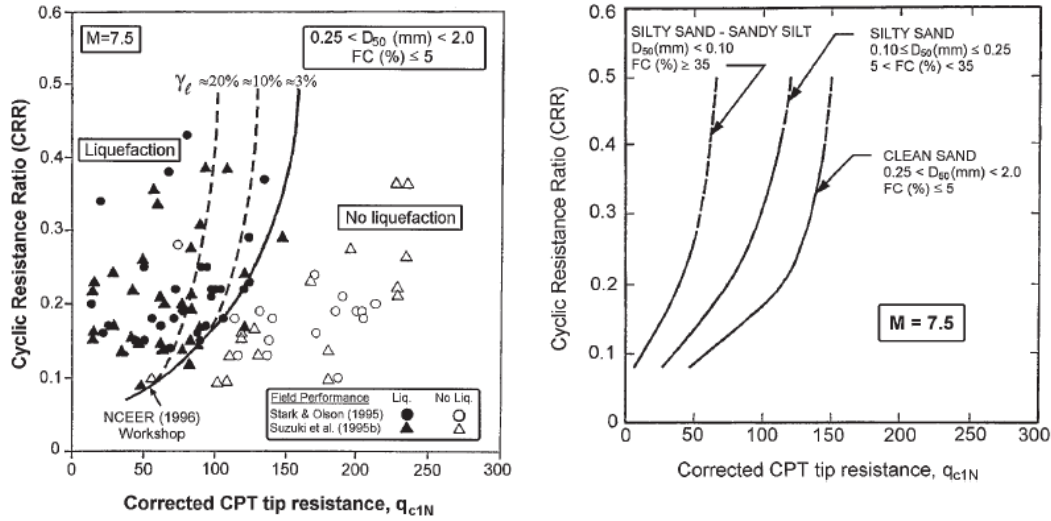
Figure 3. CRR versus corrected CPT tip resistance for a magnitude 7.5 earthquake

(Robertson and Wride, 1998).

2.1.3 Determining Factor of Safety Using Shear Wave Velocity

Penetrating methods, however, may not be reliable in certain soils and cannot be
conducted in areas such as landfills (Andrus *et al.*, 2003). Shear wave velocity is "an
engineering property that is directly related to small-strain shear modulus (Andrus *et al.*,
2003)." It is also necessary for the analysis of dynamic soil response. Due to the
correlation between the density of a soil and the shear wave velocity of a medium, CRR
and FS can be analyzed using shear wave velocity data (Song and Mikell, 2013).

The CRR is calculated using the equation,

$$CRR = 0.022(\frac{v_{s1}}{100})^2 + 2.8\left(\frac{1}{v_{s1}^* - v_{s1}} - \frac{1}{v_{s1}^*}\right) \qquad (40)$$

where v_{s1} is the overburden-stress corrected shear wave velocity and v_{s1}^* is the limited
upper value of v_{s1} for liquefaction occurrence (Song and Mikell, 2013).The overburden-
stress corrected shear wave velocity is calculated using the equation,

$$V_{s1} = V_s(\frac{P_a}{\sigma_{vo'}})^{0.25} \qquad\qquad (41)$$

where P_a is the atmospheric pressure, i.e. 100 kPa (Song and Mikell, 2013).

Figures 4a though 4c are CRR curves for a 7.5 magnitude earthquake in Holocene-age sands with FC $\leq$ 5%. Figure 4a compares CRR with SPT blow count, Figure 4b compares CRR with the CPT tip resistance, and the Figure 4c compares CRR with shear-wave velocity (Andrus *et al.*, 2003). The general shape of the curve produced by the SPT and CPT methods are similar. The curve generated by the SPT method is less conservative than the CPT and shear wave method between the blow count values eight and twenty (Andrus *et al.*, 2003). The curve generated by the CPT method is less conservative than the SPT and shear wave method above a corrected CPT tip resistance value of 120 (Andrus *et al.*, 2003). This study will further compare the results of the CPT method to the shear-wave velocity method by analyzing data from Northern Mississippi.
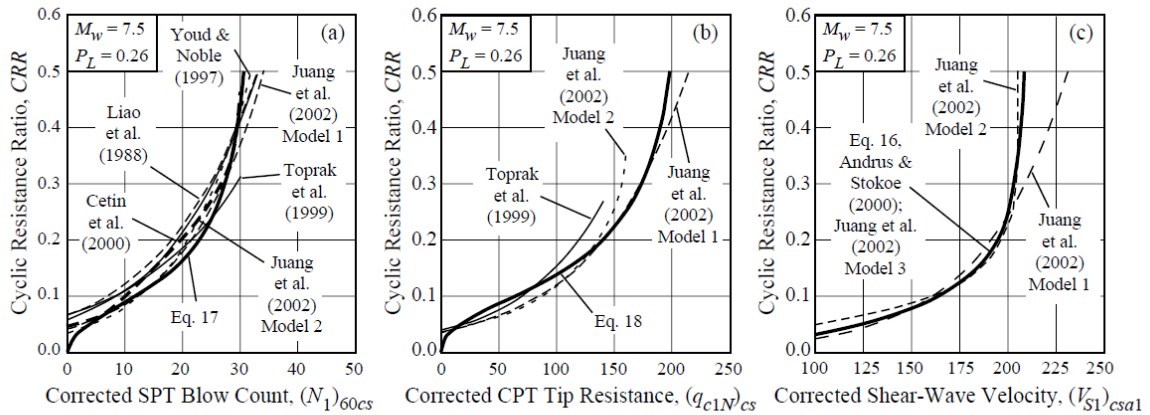

Figure 4. Graphs of **a)** corrected SPT blow count, **b)** corrected CPT tip resistance, and **c)** corrected shear-wave velocity (Andrus *et al.*, 2003).

3.0 Northern Mississippi Delta Data

A liquefaction susceptibility study of Desoto, Tunica, and Tate County, Mississippi was conducted by Dr. Chung R. Song and Nathan Mikell from the University of Mississippi Civil Engineering Department. This study will closely follow their report.

The study area is located in the Mississippi Embayment (Guo, 2014). Figure 5 is a geologic map of the area. The gray area outlines the Mississippi Delta which consists of alluvium, consisting of loam, sand, gravel, and clay, deposited by the Mississippi River (MDEQ, 2011). Tunica and part of Desoto County are within this boundary. The Kosciusko Formation is found in majority of Desoto and Tate County. The Kosciusko Formation consists of Tertiary bedded sand, clay, and some quartzite (MDEQ, 2011). The study area mainly consists of a sequence of unconsolidated sediments (Guo, 2014).
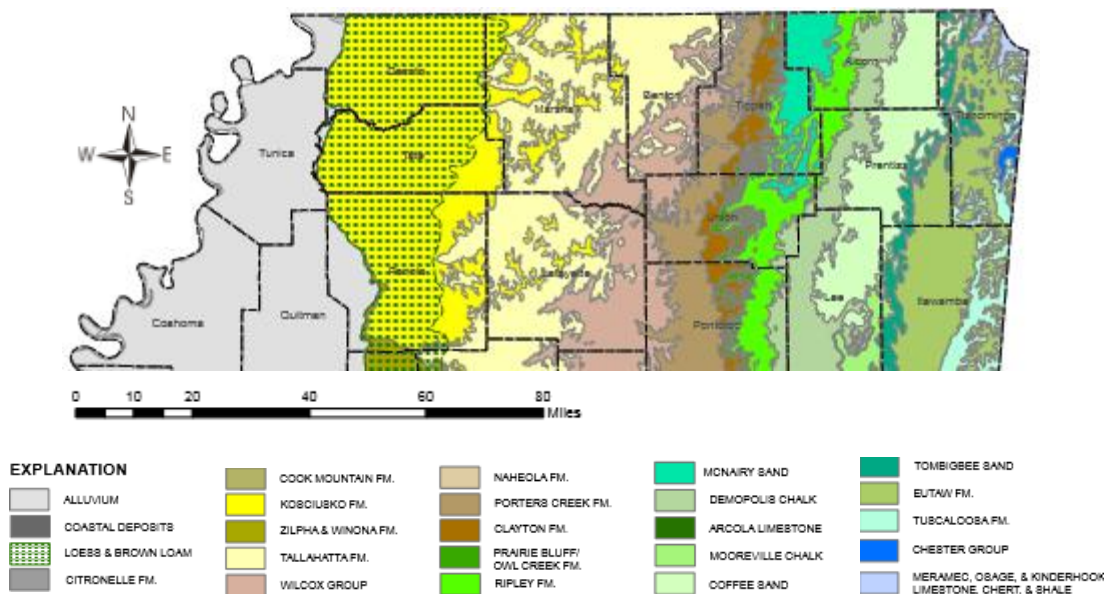

Figure 5. Geologic map of North Mississippi (MDEQ, 2011).

The preliminary data of the study area showed a wide distribution of loose sand

layers.   A sieve analysis test was conducted on sand boil samples. Depending on the

gradation, this test can sometimes give clues to a soil's liquefaction potential. A sieve

analysis test is conducted by running samples through multiple sieves with a known

screen size. The top sieve screen has the largest holes and the bottom most sieve has the

smallest hole size. Figure 6 shows the graph of grain size distribution with the percent

finer as the y-axis and the particle size in millimeters as the x-axis. The colored lines

represent the size distribution of the three samples, the dashed lines represent liquefiable

soil, and the solid black lines indicate the range typically associated with very liquefiable

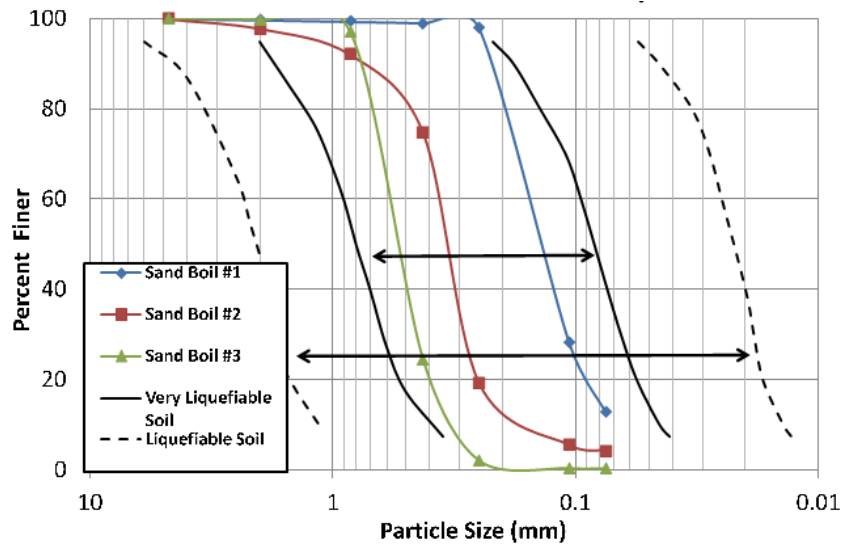soil. All three samples fall within the very liquefiable range.

Figure 6. Grain size distribution of samples and limits for liquefaction potential

(Song and Mikell, 2013).

Multiple test methods were used to evaluate the liquefaction potential. Song and

Mikell (2013) used shear wave velocity and Cone Penetration Test to evaluate

liquefaction potential. Figure 7 is a map of the borehole locations. The CPT logs from 60

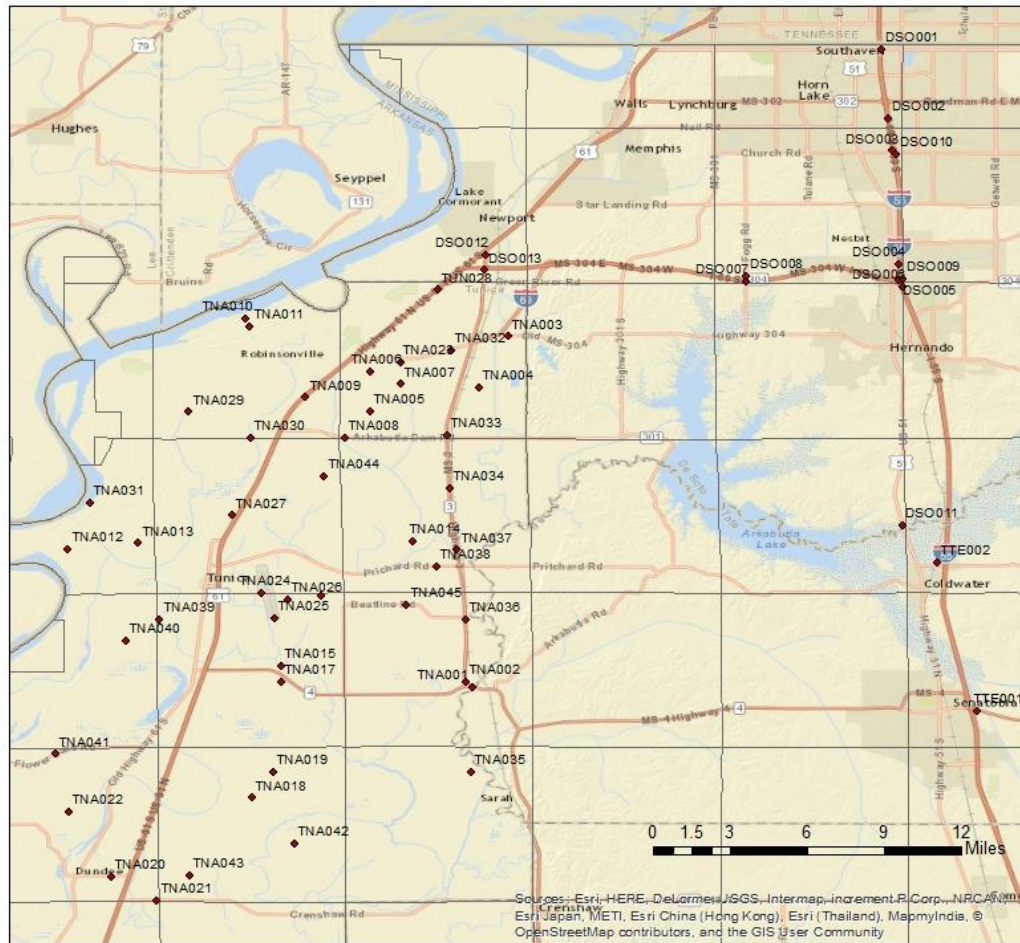boreholes in Tate, Desoto, and Tunica County were analyzed (Figure 8).

Figure 7. Borehole locations in Tate, Desoto, and Tunica County.
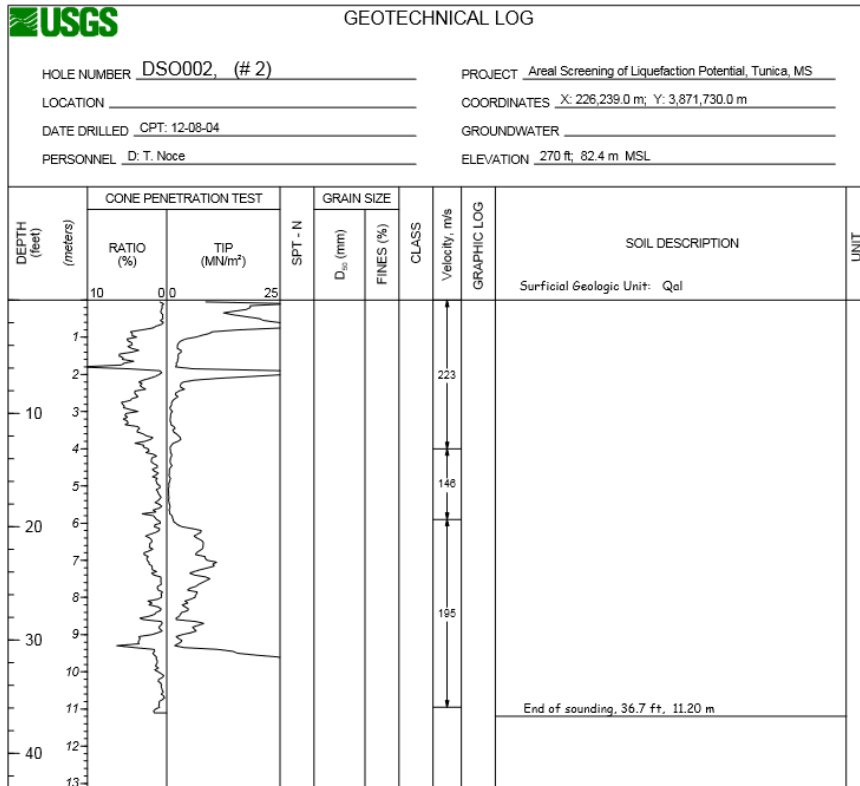
Figure 8. Sample data used in this study (Song and Mikell, 2003).

Song and Mikell (2013) created LPI maps using the approach described in section 2.2 and 2.2.2 and 2.2.3. Figure 9 is a map of the liquefaction susceptibility for a 7.5 magnitude earthquake using CPT data. Figure 10 is a map of the liquefaction susceptibility for a 7.0 magnitude earthquake using shear wave data. The scaling factor from Table 3 for a magnitude 7.0 earthquake is 1.19. Song and Mikell (2013) reported the majority of the study area to be very high to highly liquefiable for both CPT and shear-wave methods.

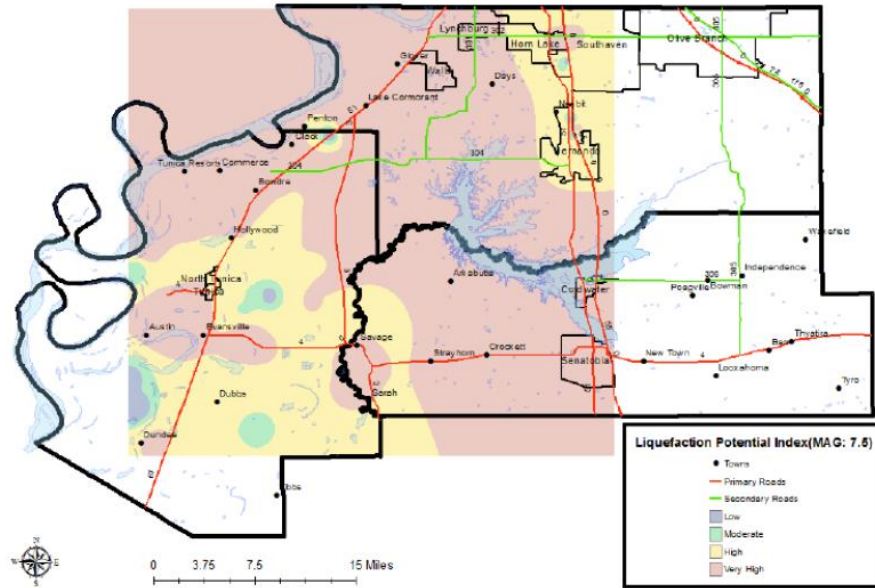**Figure 9.** Liquefaction susceptibility using CPT for a 7.5 magnitude earthquake (Song
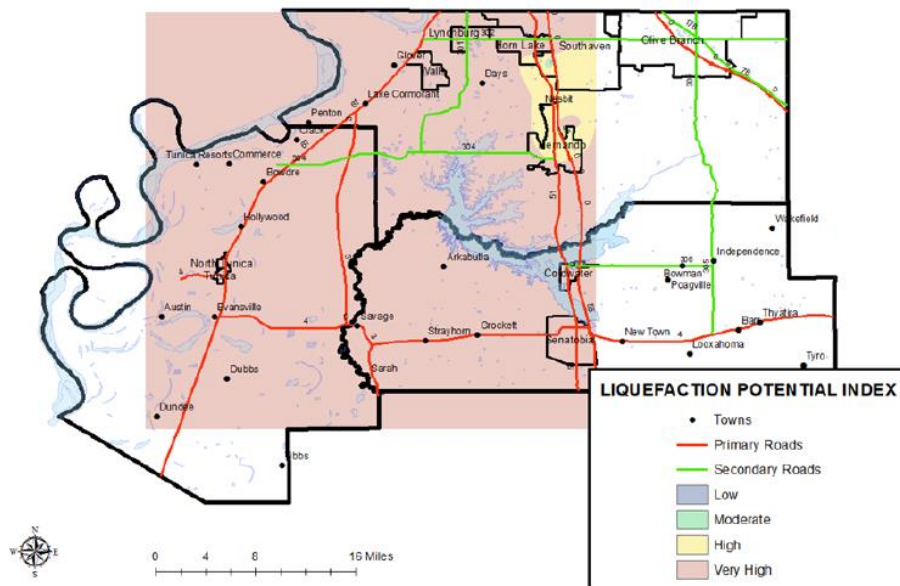
and Mikell, 2013)

Figure10. Liquefaction susceptibility using shear wave for a 7.0 magnitude earthquake

(Song and Mikell, 2013)

3.1 Reproduction of Results by Song and Mikell

This study reanalyzed and reproduced the results from the report by Song and Mikell (2013). The CSR is calculated using the method outlined in section 2.1, CRR is calculated by the method outlined in section 2.1.2 (CPT) and 2.1.3 (shear-wave velocity). The following assumptions were made while calculating the CSR:

1. The water table is one meter as in the report by Song and Mikell.

2. The total stress is calculated by integrating the unit weight over the depth.

3. The a_{max} value for North Mississippi is 0.2g, as determined by the PGA map (Figure A-2) in section 2.1.

Song and Mikell used the flow chart in Figure 11 to calculate the CRR using the CPT method. The following deviations from Song and Mikell (2013) were made while calculating CRR.

For I_c greater than 2.7, the steps in the flow chart are modified to fall into the same category as those that fall in between an I_c value of 2.5 and 2.7. I_c values that are above 2.7 will be non-liquefiable whether the above expression or equation 33 from section 2.1.2 is used. This assumption also generates larger K_c values which in turn leads to larger $(q_{c1N})_{cs}$ values. Due to the anomalously larger $(q_{c1N})_{cs}$ values, equation 25 was modified to have no upper bound.

$$if\, I_c \geq 2.70, \quad K_c = 6 \times 10^{-7} I_c^{16.76} \tag{42}$$

$$CRR_{7.5} = 93 \left(\frac{(q_{c1N})_{cs}}{1000} \right)^3 + 0.08, \; if\, 50 \leq (q_{c1N})_{cs} \tag{43}$$

Figure 12 is a graph of the factor of safety versus the I_c values. The assumption holds true for the boreholes in the graph with the exception of one point.
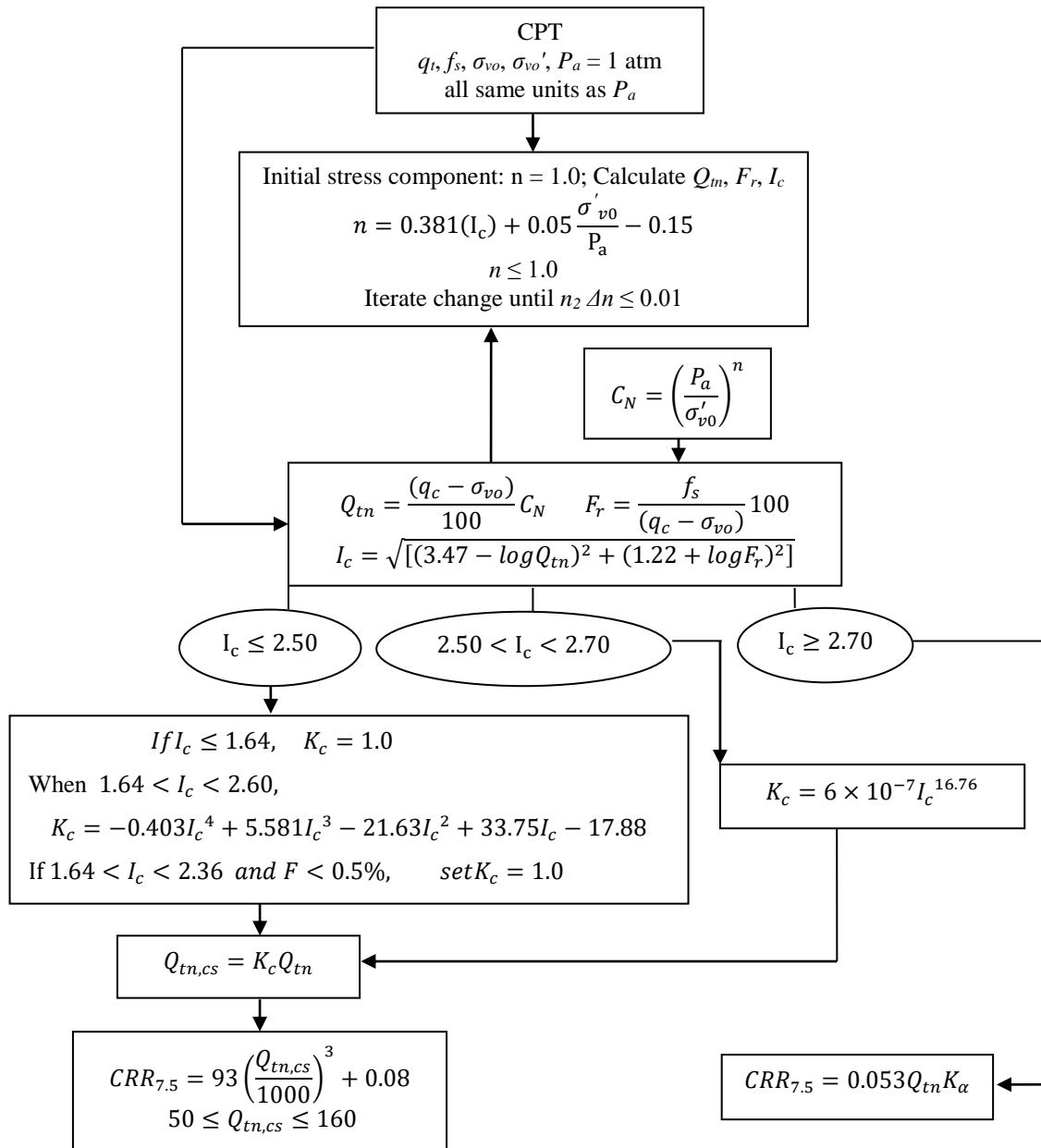
CPT
$q_t, f_s, \sigma_{vo}, \sigma_{vo}', P_a = 1$ atm
all same units as P_a

Initial stress component: n = 1.0; Calculate Q_{tn}, F_r, I_c

$$n = 0.381(I_c) + 0.05\frac{\sigma'_{v0}}{P_a} - 0.15$$

$$n \leq 1.0$$

Iterate change until $n_2 \, \Delta n \leq 0.01$

$$C_N = \left(\frac{P_a}{\sigma'_{v0}}\right)^n$$

$$Q_{tn} = \frac{(q_c - \sigma_{vo})}{100} C_N \qquad F_r = \frac{f_s}{(q_c - \sigma_{vo})} 100$$

$$I_c = \sqrt{[(3.47 - logQ_{tn})^2 + (1.22 + logF_r)^2]}$$

$I_c \leq 2.50$ $2.50 < I_c < 2.70$ $I_c \geq 2.70$

$$If \, I_c \leq 1.64, \quad K_c = 1.0$$

When $1.64 < I_c < 2.60$,

$$K_c = -0.403I_c^4 + 5.581I_c^3 - 21.63I_c^2 + 33.75I_c - 17.88$$

If $1.64 < I_c < 2.36$ and $F < 0.5\%$, $\quad set \, K_c = 1.0$

$$K_c = 6 \times 10^{-7} I_c^{16.76}$$

$$Q_{tn,cs} = K_c Q_{tn}$$

$$CRR_{7.5} = 93\left(\frac{Q_{tn,cs}}{1000}\right)^3 + 0.08$$

$$50 \leq Q_{tn,cs} \leq 160$$

$$CRR_{7.5} = 0.053 Q_{tn} K_\alpha$$

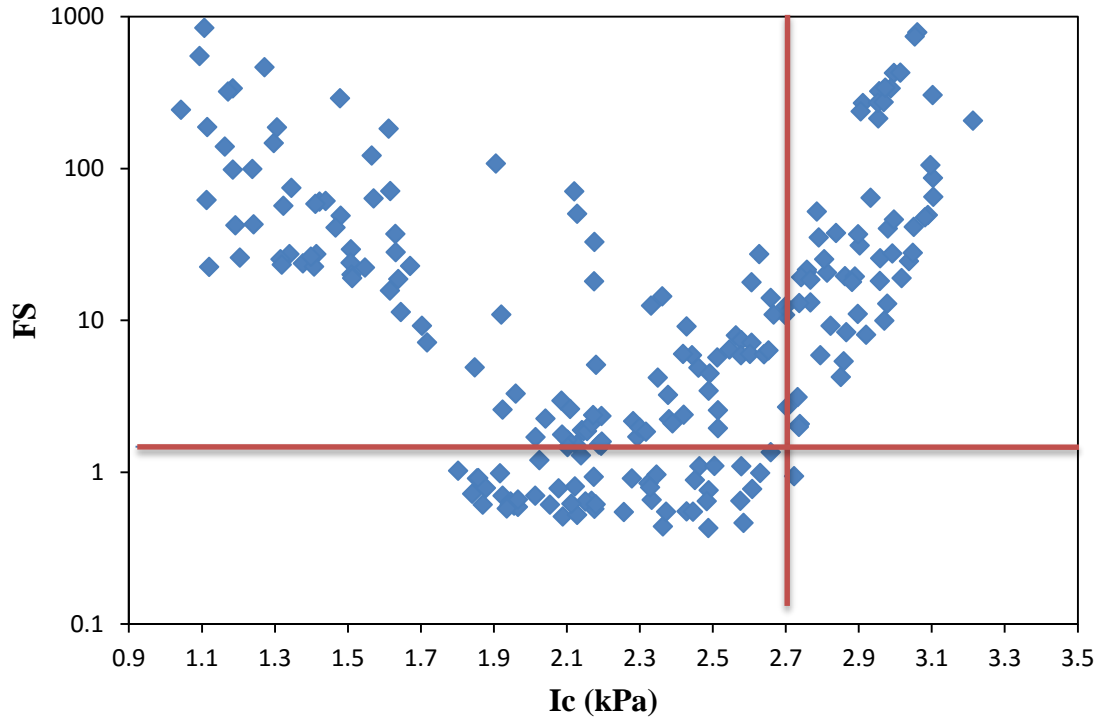**Figure 11.** Flow chart to evaluate CRR using CPT method (Robertson, 2009).

Figure 12. FS versus I_c for borehole DSO002.

The equations to calculate LPI, $w(z)$, and the F_L are modified in this report to,

$$F_L = 1 - FS \; for \; FS \leq 1 \tag{44}$$

$$F_L = 0 \quad for \; FS > 1 \tag{45}$$

$$F_L = 2.0 \times 10^6 \times e^{-18.427FS} \quad for \; 1.2 > FS \geq 0.95 \tag{46}$$

$$w(z) = 20 - 2z \tag{47}$$

$$LPI = \int_0^{10} F_L w(z) dz \tag{48}$$

because the majority of the borehole data from Song and Mikell (2013) only went to a depth of ten meters.

31

Figure 13 is a map depicting the liquefaction susceptibility of the study area. Blue represent low liquefaction, green represents medium liquefaction, yellow represents high liquefaction, and pink represents very high liquefaction. The blue circles varying in size indicate LPI values; the larger the circle, the higher the LPI. In this figure, the liquefaction potential mostly ranges from medium to high whereas in the map in Figure 8 by Song and Mikell (2013), the liquefaction potential mostly ranges from high to very high. This difference may be due to calculating total stress by integrating the unit weight, which Song and Mikell (2013) did not do. By not integrating the unit weight, the resulting total stress will be smaller. Smaller total stress values mean the soil will be more liquefiable.
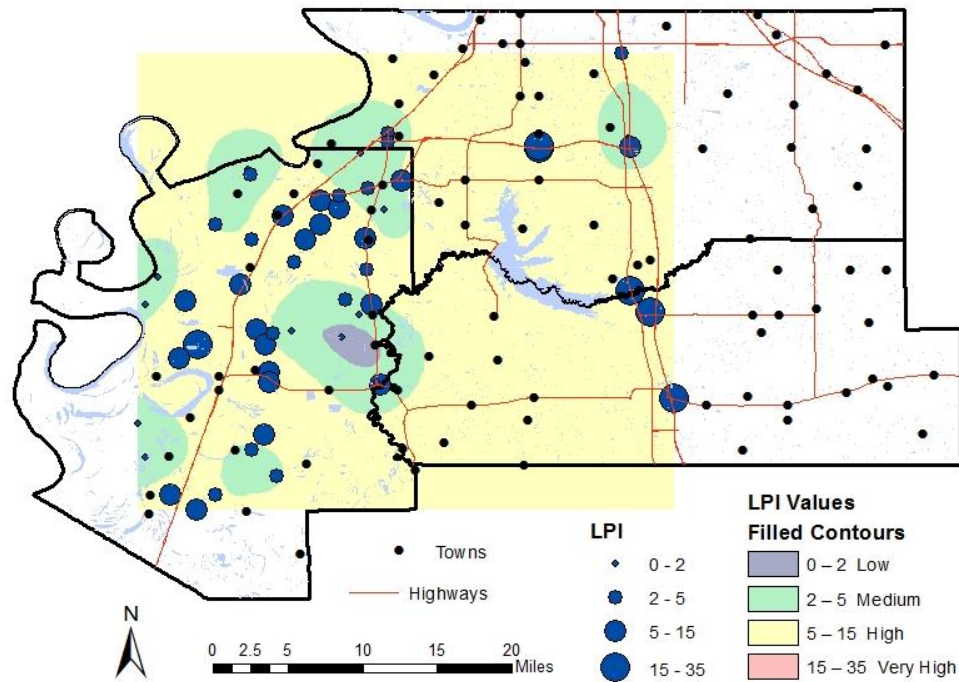

Figure 13. Liquefaction susceptibility map for a magnitude 7.5 earthquake.

3.2 Calculating LPI Using Average CSR

The purpose of this study is to create a hybrid method for calculating the LPI. It aims to combine a non-invasive and more cost effective method of calculating the CRR using surface shear wave data with and an average CSR determined using CPT data from existing boreholes.

3.2.1 Calculating Average CSR

The CSR versus depth using CPT data is calculated for all 60 boreholes. The CSR for each depth interval is averaged over all the boreholes. A standard deviation for the average CPR versus depth is calculated. Figure 14 displays the average CSR versus depth with the one standard deviation. Due to the low values of the standard deviation, this calculation indicates small viability between the individual CSR versus depth. The viability is less than 10%. An a_{max} value of 0.2g is used in calculating the CSR values because the borehole holes are located in Northern Mississippi. According to Figure 2, this area has a peak acceleration value of 20 percent. Using the average CSR works in this study appears feasible because the area is small enough that the a_{max} is the same throughout. This also indicates that the geology is fairly consistent with depth. The inconsistency in Figure 14 after a depth of 20 meters is due to the limited amount of data available past this depth.
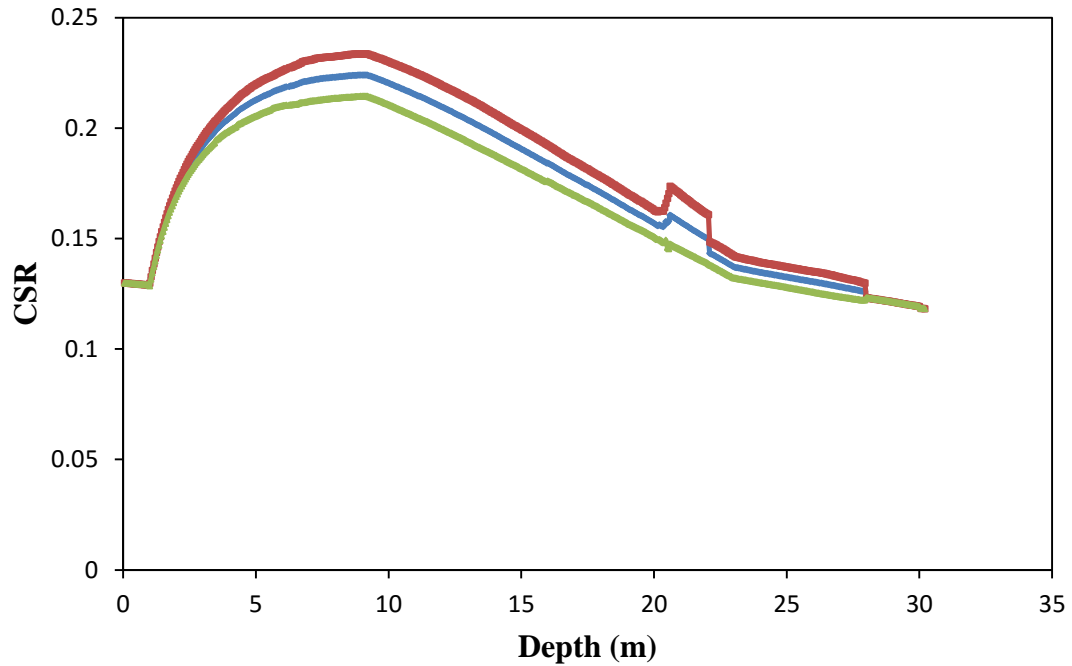
Figure 14. Graph of average CSR versus depth.

Calculations of LPI in section 2.1.2 and 2.1.3 were repeated by replacing the CSR

calculated in section 2.1.1 with the average CSR. Figure 15 illustrates the LPI values

calculated using the two methods. The data fits to a straight line with a slope of one,

indicating the similarity in the data. The liquefaction susceptibility using the average

CSR only varies slightly. All LPI values with the exception of one predicted the same

classification as those values generated using the detailed CSR calculation.
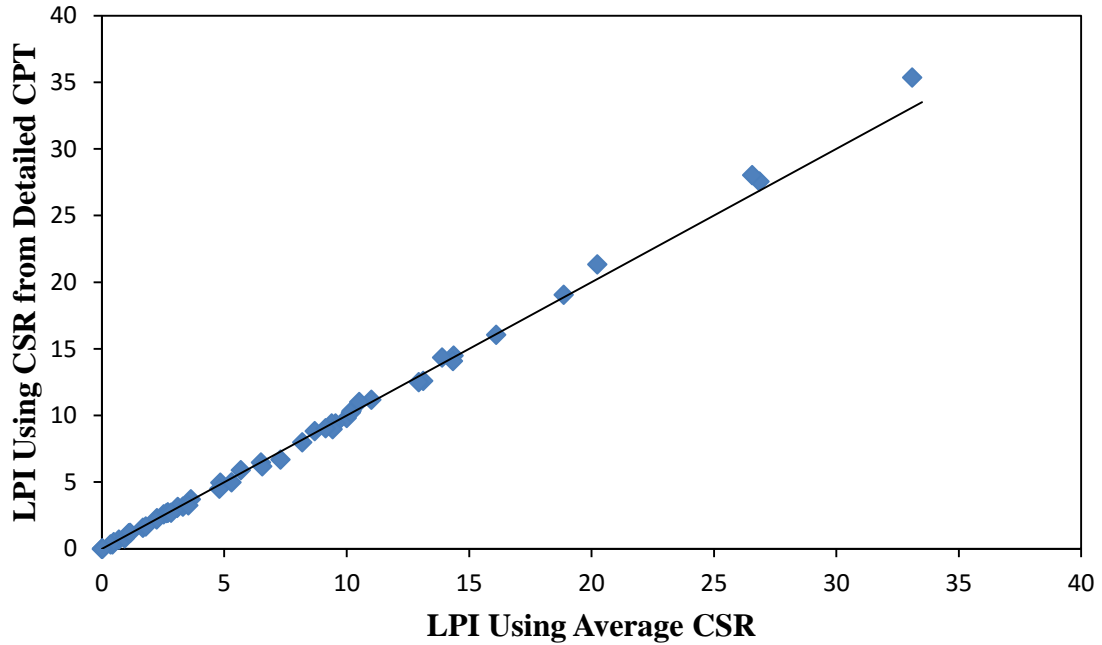
Figure 15. Comparison of LPI using detailed CPT calculation to generate CSR data and the average CSR.

3.3 Reproducing Results by Song and Mikell Using Shear Wave Data

This study attempts to reproduce the results Song and Mikell (2013) reported using shear wave data in Figure 10.The LPI is calculated using the method outlined in section2.1.3.

Equation 40 is derived in Andrus *et al*. (2000) by graphing CSR or CRR versus the overburden-stress corrected shear wave velocity calculated from equation 41(Figure 16).The lower bounding curve defines the limited upper value of V_{s1}. This figure is recreated using the average CSR values calculated in section 3.2.1 and theV_{s1} values calculated from equation 41 (Figure 17).
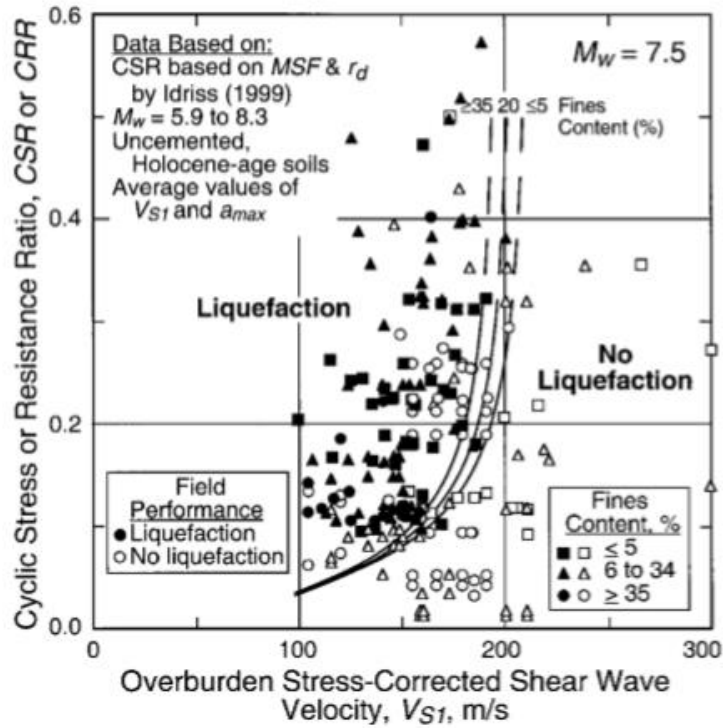
Figure 16. Graph of Cyclic Stress or Resistance Ratio versus the overburden stress-corrected shear wave velocity.
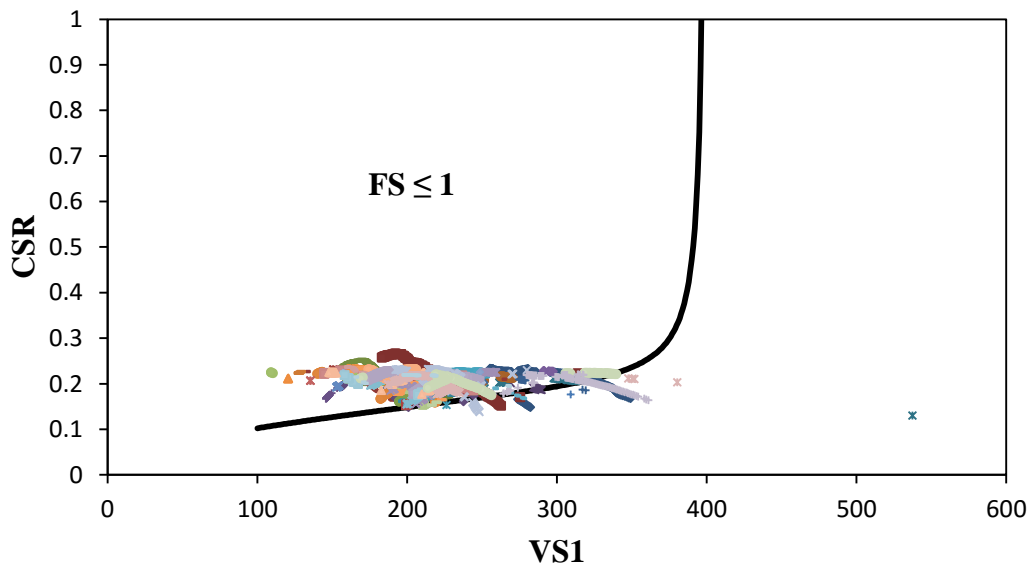

Figure 17. Graph of Cyclic Stress Ratio versus overburden stress-corrected shear wave velocity data of Northern Mississippi.

Equation 40 is modified to,

$$CRR = 0.1(\frac{v_{s1}}{100})^{0.5} + 2.8 \left(\frac{1}{v_{s1}^* - v_{s1}} - \frac{1}{v_{s1}^*}\right) \tag{49}$$

in order to fit the data for this study area.

The black curve in Figure 17represents the bounding line between liquefiable and the non-liquefiable boreholes, i.e. where the factor of safety equals one. Av_{s1}^* value of 400 m/s is determined from this graph. Figure 18 shows the relationship of the LPI values calculated from CPT data and the LPI calculated using shear wave velocity data. The LPI values calculated using shear wave data did not show a similar pattern to those calculated using CPT. Figure 19 is the frequency distribution of the LPI values. The blue bars represent the LPI using shear wave data and the red bar represents the LPI using CPT. Further study is required to understand the differences in the predicted liquefaction due to shear wave velocity and CPT.

A study done by Elnashai *et al.* (2009) and Mullen (2011) in the region allocates the majority of the study area in Tate, Tunica, and Desoto County as having a liquefaction susceptibility ranging from high to very high. The liquefaction susceptibility map was created using the method described in Youd and Perkins (1978) and an a_{max} ranging from 0.2 to 0.39g (Elnashai *et al.*, 2009). Another study done by Desai *et al.* (2004) assesses earthquake damage and liquefaction potential for Mississippi using the SPT method. A high potential of liquefaction is reported for Tunica and Desoto county using an earthquake magnitude of 7.0 (Desai *et al.*, 2004).
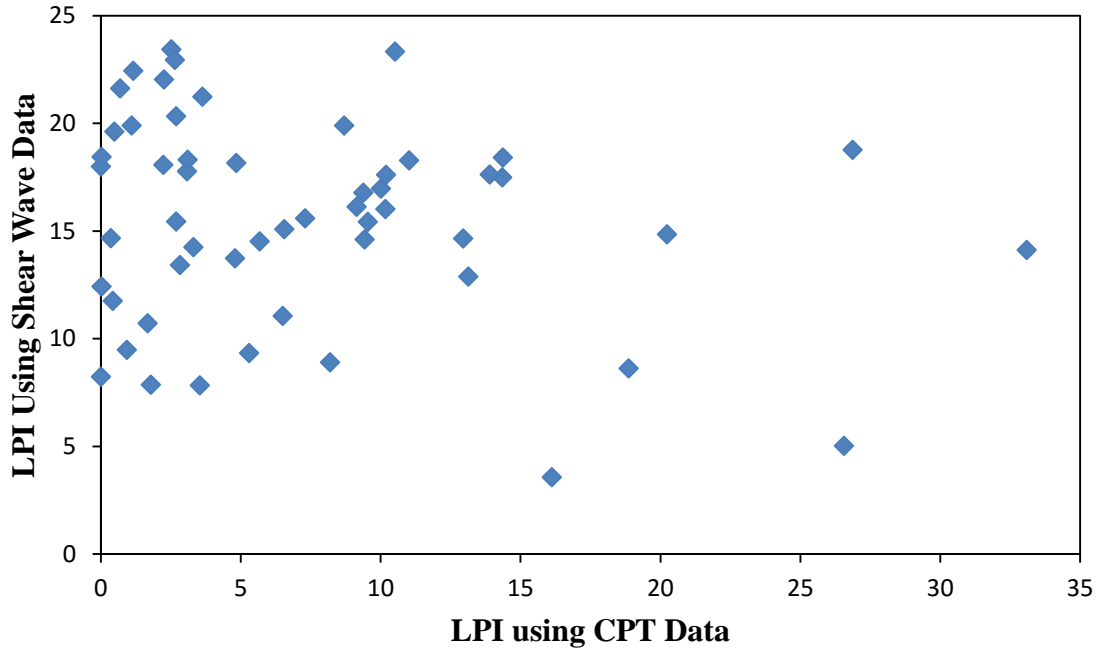
Figure 18. Graph of the liquefaction potential index using cone penetration test data versus the liquefaction potential index using shear wave velocity data.
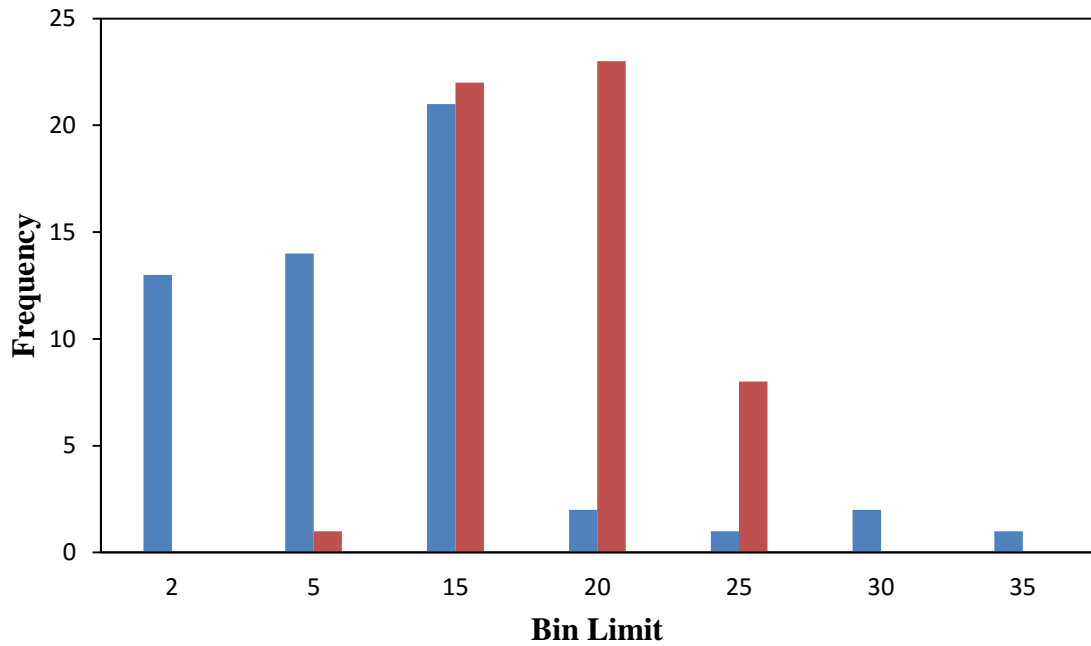

Figure 19. Frequency distribution of the liquefaction potentials using cone penetration test (red) versus using shear wave velocity (blue).

3.4 Liquefaction Potential and Vs30 Data from Shear Wave Velocity Data

The Vs30 for each borehole in the study area is calculated using equation 1.These values were then compared to the LPI values calculated using shear wave velocity. Figure 20 is a graph of LPI versus Vs30.It indicates that low velocities corresponds to higher LPI values (more liquefiable). As Table 1 indicates, low velocities in soils lead to a higher liquefaction potential.
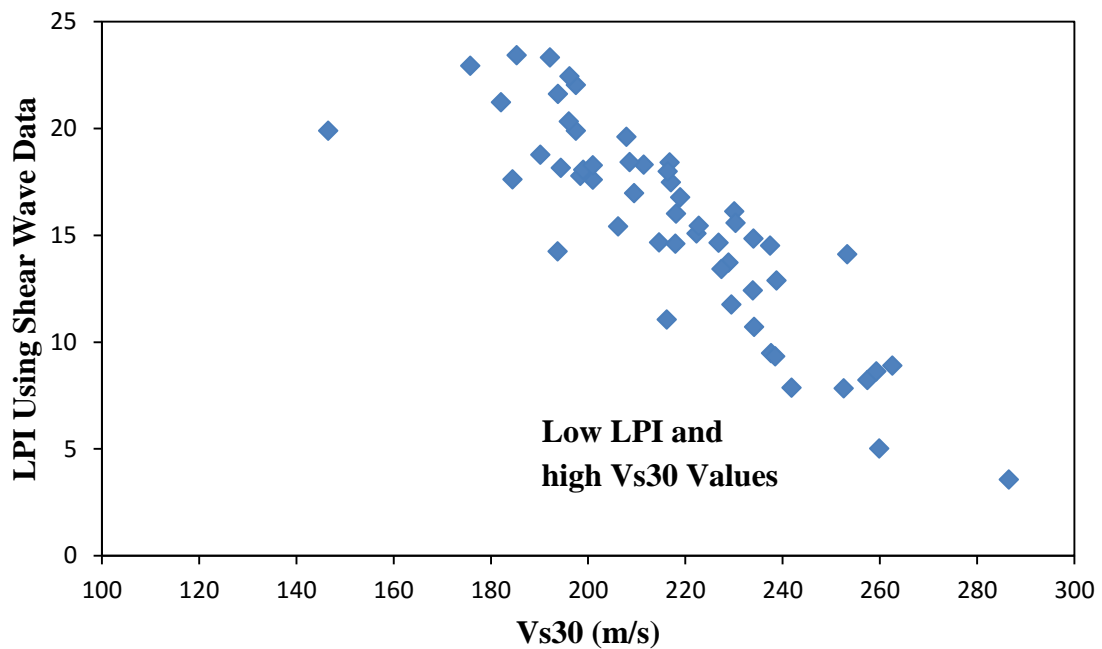

Figure 20. Liquefaction Potential Index using shear wave data versus Vs30.

4.0 Calculating Liquefaction Using Surface Shear Wave Velocity Method

Using the Multichannel Analysis of Surface Waves (MASW) method, surface
wave velocity data was collected in Tunica, Mississippi. The sample sites were in
proximity to boreholes TNA012 and TNA013 from the study of Song and Mikell (2013).
Figure 21 shows the location of data acquisition near TNA013 and Figure 22 shows the
location of data acquisition near TNA012.

Figure 21. MASW survey near borehole TNA013.

Figure 22. MASW survey near borehole TNA012.

Surface shear waves were collected at both sites using 96, 10 Hz vertical component geophones in a linear array with one meter spacing. Wave energy was created by striking a metal plate with an eight pound hammer at a 12 meter spacing interval. The source location was moved from 48 meters away from the first geophone location to 48 meters away from the final geophone. The sample time interval was 0.125 ms and the record length was 2 seconds.

The data collected was analyzed to produce a series of dispersion curves and an average shear wave versus depth profile using the SeisImager program. Figure 23 shows a selection of different dispersion curves measured using different common mid-point gathers near borehole TNA013. The average dispersion curve is used to calculate an average shear wave velocity profile and is shown in Figure 24 along with the shear wave profile for the borehole. The dispersion curve sand the average shear wave versus depth profile for the site near borehole TNA012 is shown in Figure 25 and 26, respectively.

Figure 23. Dispersion curves produced by data near borehole TNA013.
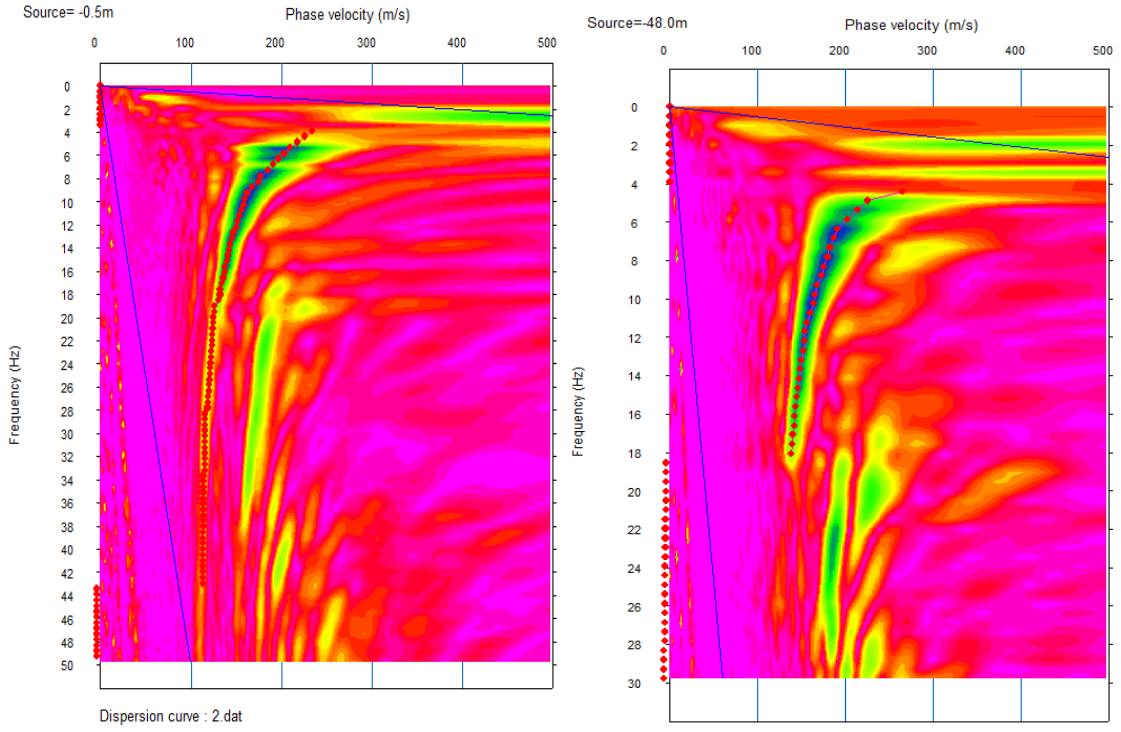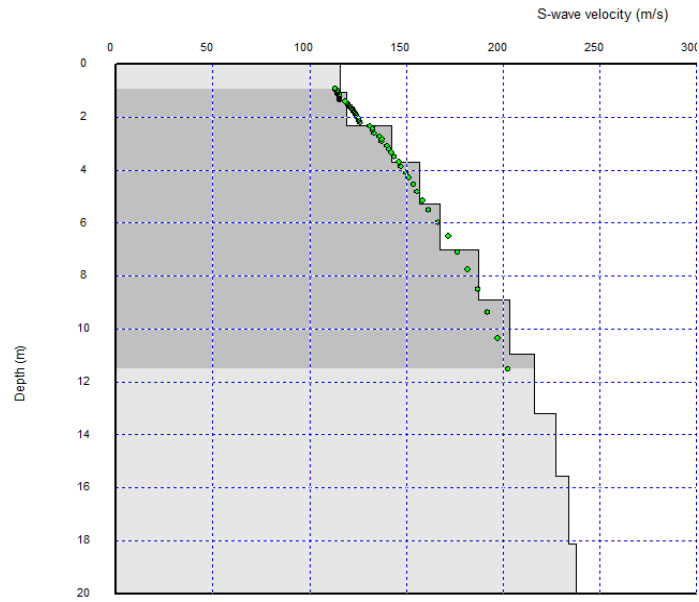

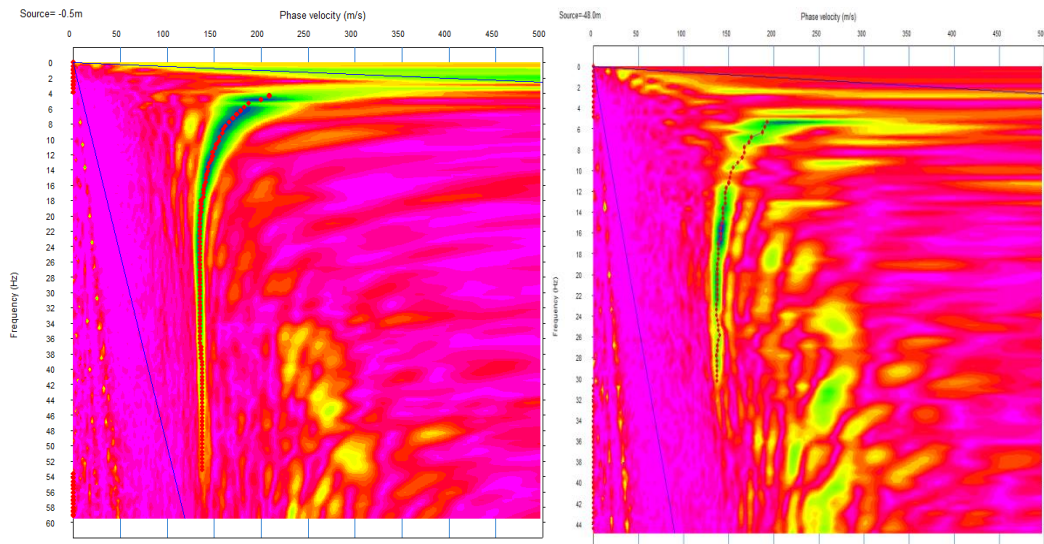**Figure 24.** Shear wave profile near borehole TNA013.

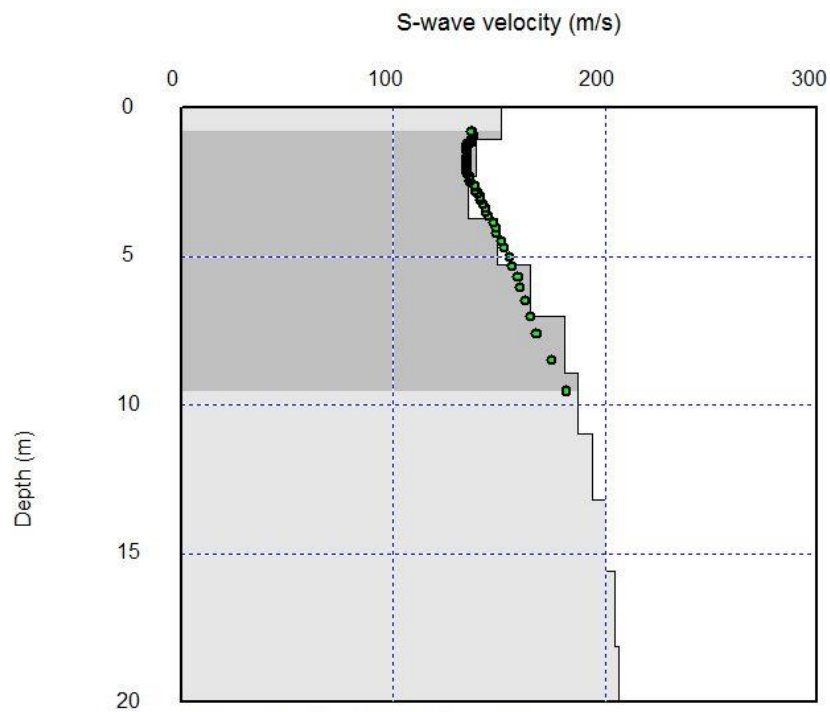**Figure 25.** Dispersion curves produced by data near borehole TNA012.

Figure 26. Shear wave profile near borehole TNA012.

The shear wave velocity versus depth in Figures 24 and 26 along with the average

CSR in Figure 14 are used to calculate the LPI at those two sites. Table 4 compares the

Vs30 using borehole data and MASW with the LPI using the CPT method, shear wave method, and MASW for both sites.

Table 4. Comparison of Vs30 and LPI methods between surveyed sites.

Method	Site #1 (near TNA013)	Site #2 (near TNA012)
Vs30 (MASW)	207 (m/s) (D)	186 (m/s) (E)
Vs30 (borehole)	239 (m/s) (D)	234 (m/s) (D)
LPI (CPT)	13.1 (H)	1.67 (L)
LPI (borehole shear wave)	12.9 (H)	10.8 (H)
LPI (MASW)	19.7 (VH)	20.5 (VH)

For the first site near borehole TNA013, the Vs30 calculated by MASW and borehole methods fall into the soil range D from Table 1. This soil type significantly amplifies shaking which can lead to liquefaction. The LPI calculated using the borehole shear wave method and CPT both fall into a range that is highly liquefiable. The LPI calculated by the MASW, however, indicates that this soil is very highly liquefiable. For the second site near TNA012, the Vs30 calculated using the borehole data indicates a soil type D, the Vs30 calculated using MASW indicates type E soil. This type of soil has the strongest amplification to shaking and can therefore usually be classified as very highly liquefiable. The LPI values calculated using CPT indicates low liquefaction while the borehole shear wave data indicates high liquefaction. The LPI calculated using MASW indicates a highly liquefiable soil. The variation in this borehole may be due to its location on the levee. The filler soil may have changed since the original CPTs were

collected. If the soil is newer and not as compacted, it would have a higher potential to liquefy.

5.0 Conclusion

Reproductions of the liquefaction potential maps did not match the original maps by Song and Mikell (2013). The reproduced map using CPT data had a liquefaction potential range from medium to high whereas the map Song and Mikell (2013) generated using CPT data has a range from high to very high. This may be due to a difference in calculating total stress. When calculating LPI using the CPT method, assuming I_c values above 2.7 to follow the same calculation as I_c values between 2.5 and 2.7 result in a non-liquefiable assignment of the layer. Therefore, this assumption does not change the end result of the calculation. The LPI values are similar when using the detailed CSR versus the regional CSR. This may only hold for Northern Mississippi and not all regions.

The four methods, shear wave data, MASW, Vs30, and CPT, can give varying results for the same locations. Though the CPT and shear wave methods do not agree with each other, the shear wave LPI and Vs30 methods do provide consistent descriptions of the site. Low velocities indicate high liquefaction potential. The LPI using CPT and shear wave data indicate the site near borehole TNA013 to be highly liquefiable. The VS30 from MASW and borehole shear waves for the soil at this site resulted in type D which is highly susceptible to amplification due to shaking which can lead to high liquefaction potentials. The liquefaction potential for the site near borehole TNA012 varied from low using CPT data to high and very high using borehole shear wave and MASW. The Vs30 using MASW corresponded to a soil type of E which is the strongest soil type to amplify shaking, leading to very highly liquefiable soil. The LPI using

MASW provides a more conservative estimate that indicates this site is very highly liquefiable. The variation of the liquefaction potential near this borehole may be due to its location on the levee. The soil at the location may have changed since the time the CPTs used in the study by Song and Mikell (2013) were acquired.

Northern Mississippi with all methods, however, is mostly highly liquefiable. Liquefaction susceptibility using the LPI value can be calculated using several different methods. Though non-invasive methods such as refraction and MASW are cheaper, the LPI calculation is more conservative.

BIBILIOGRAPHY

Andrus, R. D., Piratheepan, P., Ellis, B. S., Zhang, J., and Juang, C. H., "Comparing Liquefaction Evaluation Methods Using Penetration-VS Relationships." Department of Civil Engineering, Clemson University, 2003.

Andrus, R. D., Stokoe, H. K., B. S., "Liquefaction Resistance of Soil from Shear Wave Velocity." Journal of Geotechnical and Geoenvironmental Engineering, 2000.

Braile, L. W., Hinze, W. J., Keller, G. R., Lidiak, E. G., and Sexton, J. L. "Tectonic Development of the New Madrid Rift Complex, Mississippi Embayment, North America." Tectonophysics 131.1-2: 1-21. Print, 1986.

Central United States Earthquake Consortium. "Earthquake Information: New Madrid Seismic Zone." Web, 2014

Desai, K., Mullen, C., and George, K. P. "Earthquake Damage Assessment and Liquefaction Potential for the State of Mississippi." University of Mississippi, 2004.

Elnashai, A. M., Jefferson, T., Fiedrich, F., Cleveland, L. J., and Gress, T. "Impact of New Madrid Seismic Zone Earthquakes on the Central USA." Mid-America Earthquake Center. University of Illinois, 2009.

Fillingim, M. "Intraplate Earthquakes: Possible Mechanisms for the New Madrid and Charleston Earthquakes." *Intraplate Earthquakes: Possible Mechanisms for the New Madrid and Charleston Earthquakes*. University of California at Berkeley, 1999.

Geotechdata.info. "Standard Penetration Test." *Geotechdata.info*, 2013.

Greene, M., Power, M., and Youd, L. T. "Liquefaction: What It Is and What to Do about It." *Earthquake Basics* 1: 1-8. Innovative Technology Transfer Committee of the Earthquake Engineering Research Institute, 1994.

Guo, Z., Aydin, A., Kuszmaul, J. "Microtremor Recordings in Northern Mississippi." Department of Geology and Geological Engineering, University of Mississippi, 2014.

Holzer, T. L., Noce, T. E., Bennett, M. J. "Scenario Liquefaction Hazard Maps of Santa Clara Valley, Northern California." Bulletin of the Seismological Society of America, Vol. 99, No. 1, 367–381, 2009.

Iwasaki, T., Tatsuoka, D., Tokida, K., and Yasuda, S. A practical Method for Assessing Soil Liquefaction Potential Based on Case Studies at Various Sites in Japan, in Proc. 2nd Int. Conf. on Microzonation, San Francisco, 885-896, 1978.

Johansson, J. "Initiation of Liquefaction: Why Does Liquefaction Occur?" Department of Civil Engineering, University of Washington, 2000.

Johari, A., and Khodaparast, A. R. "Modeling of Probability Liquefaction Based on Standard Penetration Tests Using the Jointly Distributed Random Variables Method." Engineering Geology 158: 1-14. Print, 2013.

Lowrie, W. *Fundamentals of Geophysics*: "Seismology and the Internal Structure of the Earth." Cambridge University Press, UK, 83-63, 1997.

Missouri Department of Natural Resources. "Facts about the New Madrid Seismic Zone." Missouri Department of Natural Resources, n.d. Web, 2014.

Mississippi Department of Environment Quality. Geologic maps and data for Mississippi. MDEQ, 2011.

Mullen, C. "Seismic Vulnerability of Critical Bridges in North Mississippi." Mississippi Emergency Management Agency, 2011.

Odum, J. K. "Near Surface Shear Wave Velocity versus Depth Profiles, Vs30, and NEHRP Classifications for 27 Sites in Puerto Rico." *USGS*. U.S. Geological Survey, 2007.

Park, C. B., Miller, D. R., Xia, J., Ivanov, J. "Multichannel Analysis of Surface Waves (MASW)—Active and Passive Methods." The Leading Edge, 2007.

Rauch, A. F. "EPOLLS: An Empirical Method for Predicting Surface Displacements Due to Liquefaction-Induced Lateral Spreading in Earthquakes." Diss. Virginia Polytechnic Institute and State University, 1997.N.p.: Digital Library and Archives. Print, 1997.

Robertson, P. K. and Wride, C. E. (Fear). "Evaluating Cyclic Liquefaction Potential Using the Cone Penetration Test." Canadian Geotechnical Journal 35.3: 442-59. Print, 1998.

Robertson, P.K. and Fear, C.E., "Soil liquefaction and its evaluation based on SPT and CPT." Liquefaction Workshop, 1996.

Rodgers, J. D. "Fundamentals of Cone Penetrometer Test (CPT) Soundings." Missouri University of Science and Technology, 2004.

Silva, W. "Ground Motion and Liquefaction Simulation of the 1886 Charleston, South Carolina, Earthquake." Bulletin of the Seismological Society of America 93.6: 2717-736. Print, 2003.

Song, C. R., and Mikell, N. "Earthquake and Piping Hazard Assessment for Desoto, Tunica, and Tate County, Mississippi." Department of Civil Engineering, University of Mississippi, 2013.

Spall, H. "Earthquakes and Plate Tectonics." *Earthquakes and Plate Tectonics*. USGS, 1976.

United States Geological Survey. "Earthquake Hazards 101: The Basics." U.S. Geological Survey, 2015.

United States Geological Survey. "Earthquake Hazards 201: Technical Q&A." U.S. Geological Survey, 2014.

United States Geological Survey. "History of Earthquakes." U.S. Geological Survey, 2012.

United States Geological Survey. "Soil Type and Shaking Hazard in the San Francisco Bay Area." *Soil Type and Shaking Hazard in the San Francisco Bay Area*. U.S. Geological Survey, 2012.

Youd, T.L. and Perkins, D. M. "Mapping of Liquefaction Induced Ground Failure Potential." Journal of the Geotechnical Engineering Division, ASCE. v 104, n 4, 433-446, 1978.